Quasiclassical Trajectory Study of the $O(^3P) + CH_4 \rightarrow OH + CH_3$ Reaction with a Specific Reaction Parameters Semiempirical Hamiltonian

Diego Troya* and Elena García-Molina

Department of Chemistry, Virginia Tech, 107 Davidson Hall, Blacksburg Virginia, 2060-0212

Received: December 14, 2004; In Final Form: February 3, 2005

We present a theoretical study of the $O(^3P) + CH_4 \rightarrow OH + CH_3$ reaction using electronic structure, kinetics, and dynamics calculations. We calculate a grid of ab initio points at the PMP2/AUG-cc-pVDZ level to characterize the potential energy surface in regions of up to 1.3 eV above reagents. This grid of ab initio points is used to derive a set of specific reaction parameters (SRP) for the MSINDO semiempirical Hamiltonian. The resulting SRP-MSINDO Hamiltonian improves the quality of the standard Hamiltonian, particularly in regions of the potential energy surface beyond the minimum-energy reaction path. Quasiclassical-trajectory calculations are used to study the reaction dynamics with the original and the improved MSINDO semiempirical Hamiltonians, and a prior surface. The SRP-MSINDO semiempirical Hamiltonian yields OH rotational distributions in agreement with experimental results, improving over the results of the other surfaces. Thermal rate constants estimated with Variational Transition State Theory using the SRP-MSINDO Hamiltonian are also in agreement with experiments. Our results indicate that reparametrized semiempirical Hamiltonians are a good alternative to generating potential energy surfaces for accurate dynamics studies of polyatomic reactions.

Introduction

Quantitative studies of reaction dynamics require highly accurate potential energy surfaces. Whereas one can currently develop quantitative analytical potential energy surfaces (PESs) for triatomic reactions,[1] this task is much more complicated for reactions with larger dimensionality. Despite significant progress in tetratomic reactions,[2,3] the development of quantitative potential energy surfaces for systems beyond four atoms has been slow. There are two main difficulties in the calculation of a globally accurate PES for systems beyond four atoms. First, the computational effort required to accurately describe each degree of freedom with high-quality ab initio data is enormous. Second, obtaining a multidimensional analytic PES that reproduces ab initio data and does not present spurious behavior is far from trivial.

One alternative to generating PESs for systems with many degrees of freedom is the use of interpolation techniques.[4] These methods have proved useful in some tetratomic systems[2] and beyond. Recent work has demonstrated that very accurate surfaces for calculation of rate constants can be built with interpolation of very few high-quality ab initio points in the vicinity of the saddle point.[5,6] However, the computational expenditure needed in the calculation of dynamic properties with these types of surfaces increases dramatically with respect to conventional surfaces, as recently shown in a quasiclassical trajectory study of the $OH + D_2$ reaction.[7] Another alternative to developing reaction dynamics calculations of polyatomic systems with accurate interaction potentials is through "direct dynamics".[8] In direct-dynamics studies, the calculation of a PES is avoided altogether. Instead, the molecular forces required to solve the equations of motion are obtained directly from quantum-mechanical calculations at every integration step. A disadvantage of direct dynamics is that the large number of energy gradient calculations involved in extensive dynamics studies introduces a severe computational bottleneck when use of high-quality quantum-mechanical methods is required.

An emerging approach to generating a PES for reaction dynamics studies of multidimensional systems is to use direct dynamics with inexpensive quantum-mechanical methods, e.g., semiempirical Hamiltonians.[9] A problem associated with this strategy is that semiempirical Hamiltonians are rarely accurate enough for every reaction in all of the regions of the potential energy surface. However, the presence of adjustable parameters within the Hamiltonian offers the possibility of improving the accuracy of the method by deriving specific parameters for the reaction under consideration. Semiempirical Hamiltonians with specific reaction parameters (SRP)[10] have been used before for reaction dynamics studies.[11] In this paper, we further explore the prospect of these methods for accurate dynamics calculations of polyatomic reactions deriving an SRP semiempirical Hamiltonian for the $O(^3P) + CH_4 \rightarrow OH + CH_3$ reaction.

The $O(^3P) + CH_4 \rightarrow OH + CH_3$ reaction is of fundamental interest to the reaction dynamics and combustion communities.[12] The presence of abundant experimental information on rate constants and dynamics properties makes this system an excellent candidate to benchmark theoretical methods for reaction dynamics studies. Thus, a variety of quantum-dynamics methods has been applied to study this chemical reaction. For instance, Zhang and co-workers used the Semirigid Vibrating Rotor Target method to model the title reaction.[13] Yu and Nymann studied this reaction using the Rotating Bond Umbrella Model.[14] Palma and Clary have applied 4D methods to study the reaction dynamics and rate constants.[15−17] More recently, rather impressive full-dimensional quantum-dynamics calculations have been carried out by Huarte-Larrañaga and Manthe to determine thermal rate constants.[18] The surface developed by Espinosa-García and García-Bernáldez[19] (EG PES, hereafter) was used in those calculations. The EG PES was derived based on Variational Transition State Theory[20] (VTST) calculations of the thermal rate constants,[19] and remarkably, the accurate

* To whom correspondence should be addressed. E-mail: troya@vt.edu.

10.1021/jp044304+ CCC: $30.25
Published on Web 03/10/2005

TABLE 1: Calculated Reaction Energy and Barrier for the $O(^3P) + CH_4 \rightarrow OH + CH_3$ Reaction[a]

energy method/basis set //geometry and freq method/basis set[b]	reaction energy	reaction barrier
B3LYP/6-31G*	0.277 (0.467)	0.305 (0.485)
UMP2/cc-pVTZ	0.147 (0.323)	0.616 (0.788)
UMP2/AUG-cc-pVDZ	0.129 (0.299)	0.597 (0.765)
UMP2/AUG-cc-pVTZ	0.048 (0.225)	0.528 (0.700)
PMP2//UMP2/cc-pVTZ	0.088 (0.264)	0.493(0.664)
PMP2//UMP2/AUG-cc-pVDZ	0.123 (0.293)	0.472 (0.642)
PMP2//UMP2/AUG-cc-pVTZ	−0.009 (0.169)	0.411 (0.582)
CCSD(T)/AUG-cc-pVTZ//UMP2/cc-pVTZ	0.115 (0.291)	0.473 (0.644)
CCSD(T)/AUG-cc-pVTZ//UMP2/AUG-cc-pVDZ	0.118 (0.288)	0.466 (0.634)
CCSD(T)/AUG-cc-pVTZ//UMP2/AUG-cc-pVTZ	0.114 (0.291)	0.467 (0.639)
MSINDO	−0.342 (−0.151)	0.560 (0.698)
SRP-MSINDO	−0.020 (0.202)	0.436 (0.623)
MRCI[c]	0.061 (0.243)	0.455 (0.659)
exp[d]	0.069	

[a] Energies are in eV. Values in parentheses correspond to classical energies, i.e., without including zero-point energy. [b] MP2 calculations correlate all of the electrons. [c] MRCI+Q/CBL//CASPT2(10,10)/vtz calculations of ref 39. [d] Reference 42.

12-D quantum-dynamics calculations of the Manthe group were in good agreement with the statistical calculations.[18] This result gives evidence that the study of the $O(^3P) + CH_4 \rightarrow OH + CH_3$ reaction with VTST methods is legitimate.

Quasiclassical-trajectory calculations were used to study the reaction dynamics with a model that neglects the internal motions of the methyl fragment.[21,22] In that work, dynamics calculations with a triatomic PES derived based on ab initio data provided OH rotational distributions in agreement with experiments.[21] Although this triatomic model has been used with some success in this and other $X + CH_4$ reactions,[23,24] it misses the dynamics associated with the motions of the methyl fragment in the passage from reagents to products. Troya et al.[25−29] carried out full-dimensional trajectory calculations of the $O(^3P) + CH_4 \rightarrow OH + CH_3$ reaction at hyperthermal collision energies, such as is important in the context of materials erosion in low-Earth orbit. Several potential energy surfaces were used in those studies. The results of the EG PES were compared with direct-dynamics calculations developed with the PM3[30] and MSINDO[31] semiempirical Hamiltonians. All of the surfaces gave cross sections for the $O(^3P) + CH_4 \rightarrow OH + CH_3$ reaction at high collision energies that were in reasonable agreement with each other (within a factor of 2). However, large differences were noted in the partitioning of energy in products.

The dynamics of the $O(^3P) + CH_4 \rightarrow OH + CH_3$ reaction has also been studied with experimental approaches. Suzuki and Hirota reported that the excitation in the umbrella motion of the CH_3 product generated in the title reaction was marginal.[32] The source of $O(^3P)$ in those experiments was photodissociation of SO_2 at 193 nm. The corresponding average translational energy ($\langle E_{coll} \rangle$) in the center of mass of $O(^3P) + CH_4$ is 0.33 eV, which is below the reaction barrier. Thus, reaction was produced from the high-energy wing of the translational energy distribution of $O(^3P)$ atoms coming from SO_2 photolysis at 193 nm. McKendrick and co-workers studied the nascent rotational distributions of the OH product using laser-induced fluorescence.[33−35] $O(^3P)$ was generated is some of their experiments by photodissociating NO_2 at 248 nm. The translational energy distribution of the $O(^3P)$ resulting from NO_2 photolysis at 248 nm is quite broad. However, it can be inferred that the distribution peaks at $E_{coll} = 0.65$ eV (in the center of mass of $O(^3P) + CH_4$) from the internal state distributions of the photodissociation partner product (NO).[36]

In this work, we carry out full-dimensional trajectory calculations of the $O(^3P) + CH_4 \rightarrow OH + CH_3$ reaction using an SRP semiempirical Hamiltonian that accurately matches ab initio data. We compare the results of our trajectory calculations with experiments to calibrate the viability of optimized semiempirical Hamiltonians in accurate reaction dynamics studies.

SRP-MSINDO Surface

A. Electronic Structure Calculations. The energy and molecular properties of the stationary points of the $O(^3P) + CH_4 \rightarrow OH + CH_3$ reaction have been intensely studied throughout the years with electronic structure methods. Both monoreference[21,25,26,28,37] and multireference[38,39] wave functions have been used to estimate the reaction energy and barrier. Likely, the most accurate estimate of the saddle point properties corresponds to the recent multireference configuration-interaction (MRCI) studies by Hase and co-workers.[39]

These MRCI calculations of the stationary points were used to derive an SRP semiempirical Hamiltonian for study of alkane processing under the action of hyperthermal oxygen.[40] The main focus of that work was to generate a surface that described accurately the stationary points of the most important reaction channels of the $O(^3P)$ reactions with saturated alkanes. The reaction channels include H abstraction (to give OH + alkyl radicals), H elimination (to give H + alkoxy radicals), C−C breakage (to give alkyl and alkoxy radicals in reactions with alkanes other than methane), and ensuing secondary and unimolecular dissociation reactions. Our efforts are focused on generating a specific reaction parameters Hamiltonian that is accurate only for the $O(^3P) + CH_4 \rightarrow OH + CH_3$ reaction. However, our goal is to develop an accurate Hamiltonian in all of the regions of the potential energy surface explored in low-energy reaction dynamics studies (reaction swath), and not only in the stationary points.

Table 1 shows the title reaction energies and barriers calculated with a variety of semiempirical and ab initio methods. The ab initio calculations have been carried out with the GAUSSIAN 03 suite of programs.[41] The data shown in the table are expected to be less accurate than earlier calculations. Nevertheless, we study the performance of less accurate methods to identify electronic-structure techniques that can provide a good description of the reaction swath at a reasonable computational cost. Density functional calculations (B3LYP/6-31G*) overestimate the experimental[42] reaction energy and underestimate the barrier as predicted by more accurate methods. Unrestricted second-order Møller−Plesset calculations (UMP2) with correlation-consistent basis sets slightly overestimate the reaction energy and barrier. However, spin-projection of the UMP2 wave function[43] (PMP2 calculations) results in a better agreement with the experimental reaction energy, and with

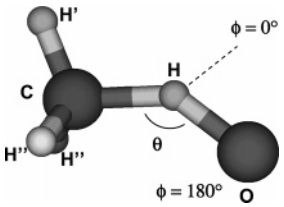

Figure 1. Definition of the O−H−C angle (θ) and dihedral angle (ϕ) used to scan the potential energy surface of the $O(^3P) + CH_4 \rightarrow OH + CH_3$ reaction.

higher quality calculations. Coupled-cluster energy calculations based on UMP2 geometries are shown to be chemically accurate when compared with experiments and MRCI calculations. Regarding the basis sets, we observe that CCSD(T)/AUG-cc-pVTZ single-point energies calculated from geometries obtained at the UMP2 level with the AUG-cc-pVDZ, cc-pVTZ, and AUG-cc-pVTZ basis sets are very close to each other. This means that the differences in geometry emerging from these three basis sets are minor. In addition, the least expensive of these basis sets (AUG-cc-pVDZ) provides satisfactory results when used with the PMP2 method. Thus, the PMP2//UMP2/AUG-cc-pVDZ combination is the one with the best accuracy/computational expenditure ratio among those studied here. Likely, the good performance of this method/basis set combination is due to a cancellation of the errors stemming from the incompleteness of the basis set and the incapability of second-order Møller−Plesset methods to completely account for all of the electronic correlation. Notwithstanding, we have used PMP2//UMP2/AUG-cc-pVDZ calculations to study the global potential energy surface of the $O(^3P) + CH_4 \rightarrow OH + CH_3$ reaction beyond the stationary points and the minimum energy reaction path. The ultimate goal of this ab initio study is to produce a dense grid of data points that will serve as a benchmark to calibrate the performance of the MSINDO semiempirical Hamiltonian.

Our ab initio study of the potential energy surface is based on relaxed scans of the O−H distance in the region of the surface connecting reagents with the saddle point, and of the C−H distance in the region of the surface connecting products with the saddle point. We perform relaxed scans fixing different O−H−C angles (θ), and 180° or 0° O−H−C−H′ dihedral angles (ϕ). (The definition of ϕ and θ is shown in Figure 1.) The OH distance is scanned starting from ∼2.2 Å until the saddle point region. Scans are carried out fixing the θ angle at 180°, 170°, 160°, 150°, 140°, 130°, 120°, and 110°, and fixing the dihedral angle ϕ at 180°. The rest of the coordinates of the system are optimized. The C−H distance is scanned starting from 2.56 Å until the saddle point region at the same O−H−C angles, and $\phi = 180°$ dihedral angle. A subset of calculations is performed for $\phi = 0°$. Overall, we have calculated 728 points at the PMP2//UMP2/AUG-cc-pVDZ level to describe the $O(^3P) + CH_4 \rightarrow OH + CH_3$ reaction swath in the 0−1.30 eV potential energy region. The computational effort associated with these calculations was roughly two weeks of CPU time. We note that our grid of ab initio points in the low-energy region of the PES is ∼50 times more dense than that used in the derivation of the triatomic potential energy surface mentioned above, which contained 35 points.[21] In the following, we describe how we use this grid of points to improve the accuracy of the MSINDO semiempirical Hamiltonian.

B. Derivation of MSINDO Specific Reaction Parameters. Table 1 shows that the original MSINDO semiempirical Hamiltonian describes the energy barrier reasonably well, but fails to describe the reaction energy. To improve the performance of the MSINDO semiempirical Hamiltonian for the $O(^3P) + CH_4 \rightarrow OH + CH_3$ reaction, we have reoptimized the original set of parameters using the grid of points calculated at the PMP2//UMP2/AUG-cc-pVDZ level. Our optimization routine is based on a nonlinear least-squares algorithm obtained from the minpack libraries.[44] All of the parameters of the O, H, and C atoms included in the MSINDO Hamiltonian (except the ones describing bonding to third-row elements) are optimized to minimize the root-mean-square deviation between the semiempirical and ab initio energies.

TABLE 2: Original Set of MSINDO Parameters for the H, C, and O Atoms, and Specific Reaction Parameters for the $O(^3P) + CH_4 \rightarrow OH + CH_3$ Reaction

	H		C		O	
	original	SRP	original	SRP	original	SRP
			orbital exponents			
ξ_s^U	1.0060	1.1571	1.6266	1.6506	2.1109	2.1253
ξ_p^U			1.5572	1.5350	1.9055	1.8921
ξ_s	1.1576	1.1532	1.7874	1.7001	2.3538	1.9626
ξ_p			1.6770	1.5211	2.1559	2.1612
			valence-state ionization potentials			
I_s	0.5000	0.4027	0.8195	0.7798	1.6838	1.7486
I_p			0.3824	0.3942	0.5780	0.5944
			pseudopotential parameters			
$-\epsilon_{1s}$			10.4300	11.0696	19.5500	20.8504
τ_{1s}			5.0830	4.9745	7.3271	6.9331
			resonance integral parameters			
K_σ	0.1449	0.1581	0.0867	0.0925	0.1242	0.1241
K_π			0.0478	0.0334	0.0760	0.0494
k_1	0.3856	0.3963	0.4936	0.4895	0.2485	0.2473
k_2	0.5038	0.4680	0.6776	0.4667	0.2246	0.1655

The initial MSINDO set of parameters and the set that best matches ab initio calculations for the $O(^3P) + CH_4 \rightarrow OH + CH_3$ reaction (SRP-MSINDO parameters) are shown in Table 2. The optimized set of parameters provides very good descriptions of the reaction energy and barrier (see Table 1), and other regions of the potential energy surface. The most remarkable improvement of the SRP-MSINDO Hamiltonian is in the reaction energy. The standard MSINDO Hamiltonian predicts that the $O(^3P) + CH_4 \rightarrow OH + CH_3$ reaction is notably exothermic (see Table 1). However, experiments and calculations indicate that the reaction is nearly thermoneutral. The optimized set of parameters corrects the deficiencies in the description of the reaction energy by the standard set, and is able to reproduce highly accurate calculations and experiments.

Figure 2 illustrates the improvement to the MSINDO Hamiltonian for regions of the potential energy surface away from the minimum energy reaction path. In the figure, the energies of the MSINDO and SRP-MSINDO semiempirical Hamiltonians are compared with PMP2//UMP2/AUG-cc-pVDZ data for relaxed scans of the C−H and O−H distances. The scans in Figure 2a−d are focused on the characterization of the region of the PES connecting the saddle point with products. The SRP-MSINDO method reproduces quite remarkably the ab initio data, improving over the original MSINDO Hamiltonian. Parts e and f of Figure 2 show relaxed scans of the O−H distance that describe the region of the surface connecting reagents with the saddle point. Both the original MSINDO and SRP-MSINDO Hamiltonians describe this region reasonably well. However, the performance of the SRP-MSINDO method is superior. For instance, Table 1 shows that the reaction barrier calculated with the SRP-MSINDO Hamiltonian accurately matches MRCI calculations. Overall, the root-mean-square deviation between the energies provided by the optimum set of MSINDO parameters and the ab initio energies is 2.5 times smaller than

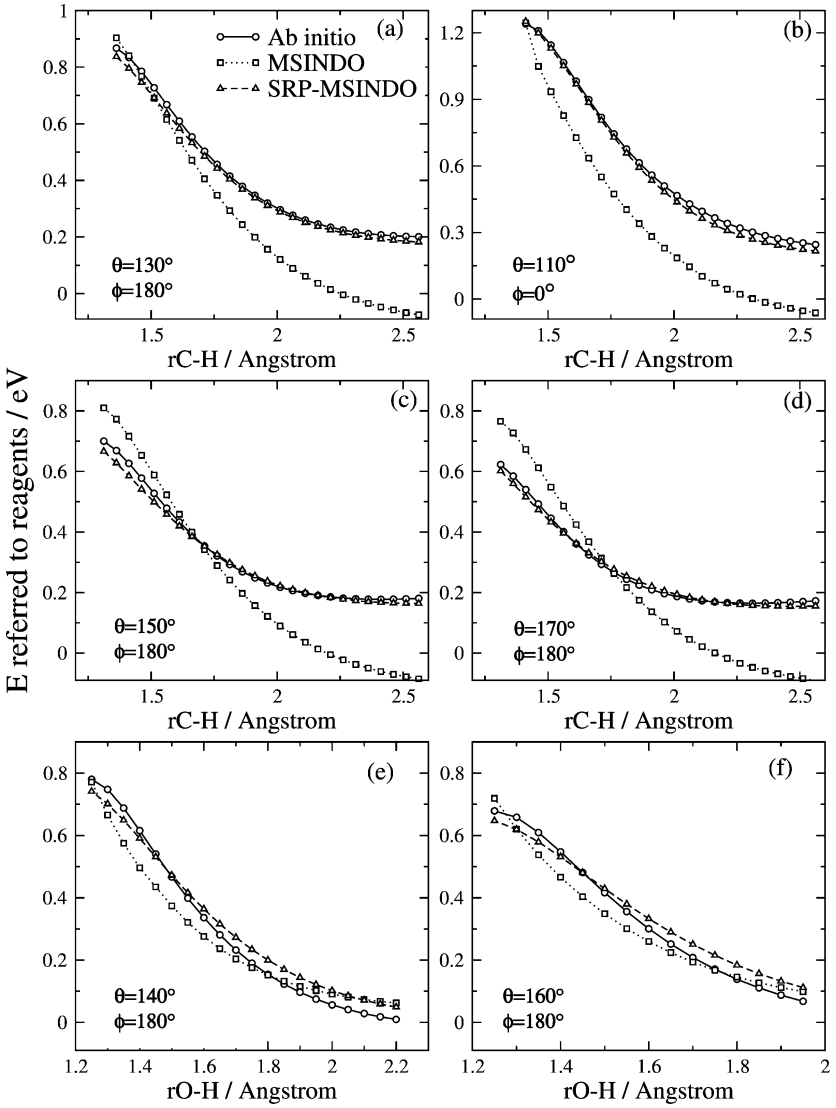

Figure 2. Comparison of the energies of MSINDO and SRP-MSINDO semiempirical Hamiltonians with PMP2//UMP2/AUG-cc-pVDZ data for the $O(^3P) + CH_4 \rightarrow OH + CH_3$ reaction. The energy curves correspond to relaxed scans of the C−H distance from the region of the saddle point to products (panels a, b, c, and d) and the O−H distance from reagents to the saddle point (panels e and f). The O−H−C and H′−C−H−O angles are fixed. (a) $\theta = 130°$, $\phi = 180°$; (b) $\theta = 110°$, $\phi = 0°$; (c) $\theta = 150°$, $\phi = 180°$; (d) $\theta = 170°$, $\phi = 180°$; (e) $\theta = 140°$, $\phi = 180°$; (f) $\theta = 160°$, $\phi = 180°$.

TABLE 3: Geometries of the $^3A''$ Saddle Point of the $O(^3P) + CH_4 \rightarrow OH + CH_3$ Reaction[a]

method/basis set	$R_{CH''}$	$R_{CH'}$	R_{CH}	R_{OH}	∠CHO	∠H′CHO
B3LYP/6-31G*	1.089	1.088	1.389	1.147	177.1	180.0
MP2/AUG-cc-pVDZ	1.094	1.094	1.265	1.221	179.3	180.0
MP2/AUG-cc-pVTZ	1.081	1.080	1.242	1.224	179.3	180.0
SRP-MSINDO	1.103	1.103	1.237	1.232	179.4	180.0
MSINDO	1.075	1.075	1.261	1.136	179.2	180.0

[a] Distances are in angstrom and angles in degrees. See Figure 1 for the definition of the coordinates. All of the calculations have been performed with unrestricted wave functions.

the root-mean-square deviation with the original set (0.063 and 0.160 eV, respectively).

Table 3 shows the saddle point geometries of the $O(^3P) + CH_4 \rightarrow OH + CH_3$ reaction with different electronic structure methods. As described in prior studies,[37] there are two surfaces of triplet multiplicity correlating reagents and products in the ground state. The saddle points of both surfaces have C_s symmetry, and are nearly degenerate. In this work, we are concerned with the ground-state surface, and therefore Table 3 shows the geometry of the $^3A''$ saddle point. Calculations with the MP2 method indicate that the C−H distance of the bond that is being broken is ∼15% larger than that in reagents, and the O−H distance that is being formed is ∼25% larger than that in products. On the other hand, B3LYP/6-31G* calculations predict a transition state with an enhanced "late" character. The B3LYP C−H distance of the saddle point is ∼25% larger than that in reagents and the O−H distance is only 15% larger than that in products. The saddle-point structure of the original MSINDO Hamiltonian exhibits an O−H distance that is too short. The optimized SRP-MSINDO Hamiltonian corrects this defect with the MSINDO surface, bringing the geometries of the saddle point closer to MP2 estimates. This is an interesting result because geometries were not explicitly included in the derivation of the SRP-MSINDO Hamiltonian.

Summarizing, we have reoptimized the parameters of the MSINDO semiempirical Hamiltonian to reproduce ab initio calculations of the $O(^3P) + CH_4 \rightarrow OH + CH_3$ reaction. In the following, we calibrate the performance of the SRP-MSINDO surface based on kinetics and dynamics calculations.

TABLE 4: Calculated and Experimental Thermal Rate Constants for the $O(^3P) + CH_4 \rightarrow OH + CH_3$ Reaction[a]

T/K	CVT EG PES[b]	ICVT SRP MSINDO	CVT/μOMT EG PES[b]	ICVT/μOMT SRP MSINDO	exptl[c]	exptl[d]
200	7.1×10^{-23}	2.1×10^{-22}	8.5×10^{-21}	8.6×10^{-20}		
250	1.5×10^{-20}	3.4×10^{-20}	5.3×10^{-19}	1.3×10^{-18}		
300	5.3×10^{-19}	1.0×10^{-18}	8.7×10^{-18}	1.0×10^{-17}	9.0×10^{-18}	$5.5(+5.5,-2.8) \times 10^{-18}$
400	5.2×10^{-17}	7.7×10^{-17}	3.3×10^{-16}	2.3×10^{-16}	3.4×10^{-16}	$3.0(+0.8,-0.7) \times 10^{-16}$
600	6.3×10^{-15}	7.2×10^{-15}	1.7×10^{-14}	1.1×10^{-14}	1.7×10^{-14}	$2.0(+0.2,-0.2) \times 10^{-14}$
800	8.2×10^{-14}	8.4×10^{-14}	1.5×10^{-13}	1.0×10^{-13}	1.5×10^{-13}	$1.9(+0.2,-0.2) \times 10^{-13}$
1000	4.3×10^{-13}	4.2×10^{-13}	6.3×10^{-13}	4.7×10^{-13}	6.0×10^{-13}	$7.7(+0.9,-0.8) \times 10^{-13}$
1500	4.8×10^{-12}	4.5×10^{-12}	5.7×10^{-12}	4.8×10^{-12}	5.0×10^{-12}	$6.0(+1.6,-1.2) \times 10^{-12}$
2000	1.9×10^{-11}	1.8×10^{-11}	2.0×10^{-11}	1.9×10^{-11}	1.8×10^{-11}	$1.9(+0.8,-0.6) \times 10^{-11}$
2500	4.6×10^{-11}	4.5×10^{-11}	4.9×10^{-11}	4.6×10^{-11}	4.2×10^{-11}	$4.2(+1.7,-1.2) \times 10^{-11}$

[a] Units are cm^3 $molecule^{-1}$ s^{-1}. [b] Reference 19. [c] Reference 45. [d] Reference 48. Values in parentheses indicate the $\pm$ error bars.

Kinetics Study

A way to test the accuracy of a PES is to evaluate thermal rate coefficients. This procedure has been widely applied to the $O(^3P) + CH_4 \rightarrow OH + CH_3$ reaction and related systems[19,21,23,24] due to the availability of experimental rate constants in a broad temperature range (300−2500 K).[45−48] Although the goal of our work is to obtain an accurate PES for dynamics calculations beyond the minimum energy reaction path (MERP), calculation of rate constants can provide insight into the global accuracy of the surface, including the MERP.

Our method of choice to calculate thermal rate constants for the title reaction with the SRP-MSINDO surface is improved canonical variational transition state theory (ICVT).[20] The legitimacy of this method for the $O(^3P) + CH_4 \rightarrow OH + CH_3$ reaction has been recently established through comparisons with accurate full-dimensional quantum-dynamics calculations with the EG PES.[18] Very good agreement was found between 12-D multiconfigurational time-dependent Hartree (MCTDH) calculations and Variational Transition State Theory rate constants including large-curvature tunneling (LCT) correction, indicating that VTST is an inexpensive but yet accurate method to calculate thermal rate constants.

Our calculations of thermal rate constants for the $O(^3P) + CH_4 \rightarrow OH + CH_3$ reaction have been carried out interfacing the SRP-MSINDO Hamiltonian with the POLYRATE 9.1 suite of programs.[49] We have calculated the MERP starting from the saddle point and going downhill to reagents and products with the method of Page and McIver.[50] Our calculations cover the reaction coordinate in the −1.9 to 1.9 $amu^{1/2}$ bohr region at 0.001 $amu^{1/2}$ bohr steps. Overall, 1800 quantum-mechanical Hessians are calculated along the minimum energy reaction path to obtain the adiabatic PES required in ICVT calculations.

Table 4 shows a comparison of the rate constants calculated in this work with previous calculations on the EG PES,[19] and with experiments.[45,48] The calculated thermal rate constants consider the microcanonical optimized multidimensional (μOMT) tunneling approach. The SRP-MSINDO surface rate constants estimated in this way agree with earlier calculations and with experiments in the temperature range where experimental information is available (300−2500 K). At 200 K, the tunneling-corrected SRP-MSINDO rate constants are larger than the EG PES ones. A reason for this discrepancy can be found in the harmonic normal-mode frequencies of the saddle point shown in Table 5. The imaginary frequency of the SRP-MSINDO PES is larger than that of the EG PES, which is a consequence of the narrower MERP of the SRP-MSINDO surface in the saddle-point region, and results in enhanced tunneling. Table 5 also shows that both PESs underestimate the values of the imaginary frequency of ab initio calculations, indicating limitations in both surfaces. In the absence of experimental information, it cannot be determined what set of calculated rate constants are more accurate at low temperatures. It is possible that the EG PES rates are more accurate because this surface was derived with the goal of matching experimental rate constants. As mentioned above, we have derived the SRP-MSINDO surface with the goal of performing dynamics calculations outside the MERP, and the grid of 728 ab initio points to which we fit our SRP-MSINDO surface mostly describes regions of the potential energy surface removed from the MERP. It is also possible that the limited level of the ab initio grid of points (PMP2/AUG-cc-pVDZ) might introduce some error in the very low-temperature rate constants. Another noticeable feature of the SRP-MSINDO calculations is the overestimation of harmonic frequencies of more accurate calculations by ∼20% (see Table 5). This pitfall with the MSINDO Hamiltonian surely influences the accuracy of the low-temperature rate constants and should be corrected in future optimizations of this method. The extent to which all of these factors play a role in the low-temperature rate constants will be determined when experiments or more accurate ab initio-based calculations become available.

TABLE 5: Normal Mode Harmonic Vibrational Frequencies (cm^{-1}) of the $^3A''$ Saddle Point of the $O(^3P) + CH_4 \rightarrow OH + CH_3$ Reaction Calculated with Different Methods

EG PES	SRP-MSINDO	UMP2/aug-cc-pvdz	CASSCF(10,10)/vtz[a]
3086	3947	3275	2971
3086	3944	3246	2966
2954	3788	3112	2956
1433	1564	1434	1407
1433	1525	1360	1333
1246	1508	1214	1187
1155	1347	1108	1074
1155	1328	1104	1060
605	779	618	515
323	424	377	366
323	368	214	167
1549i	1719i	2197i	2567i

[a] Reference 39.

Notwithstanding, the performance of the SRP-MSINDO semiempirical Hamiltonian where experimental rate constants are available is remarkable, providing rate constants that are within experimental uncertainty at most temperatures. These results suggest that one could develop SRP parameters for MSINDO or other semiempirical Hamiltonians to obtain very accurate surfaces only in the vicinity of the minimum energy path for reactions of arbitrary dimensionality.

Dynamics Study

A. Details of the Calculations. We have carried out an extensive quasiclassical trajectory study of the $O(^3P) + CH_4$

$\rightarrow$ OH + CH_3 reaction with various PESs to compare with experiments and learn about the dynamic properties of the system. Our calculations are focused on the SRP-MSINDO Hamiltonian derived in this work, but for the sake of comparison, calculations have also been performed with the original MSINDO Hamiltonian and the EG PES.

Trajectories are started at 15 au between the centers of mass of reagents, and are stopped when the O−C or an H−C internuclear distance reaches 15 au after the inner turning point of the trajectories. The initial conditions for methane are calculated with the VENUS96 code of Hase et al.[51] Zero-point vibrational energy is supplied with microcanonical sampling. We have verified in sample calculations with the EG PES that this procedure of selection of initial conditions for methane yields analogous results to providing 0.5 quanta of vibrational excitation to each vibrational mode. $RT/2$ ($T = 300$ K) rotational energy is given about each axis of the molecule.

Once the initial conditions are generated, we integrate the equations of motion with a home-designed trajectory propagation code that utilizes a Runge−Kutta−Gill 5th-order predictor and an Adams−Moulton 6th-order corrector method. The integration time step is 10 au. The self-consistent-field convergence criterion in our semiempirical direct-dynamics calculations is set to 1.0×10^{-7} hartree. Use of unrestricted wave functions in our direct-dynamics trajectories leads to small spin contamination in the region of strong interaction. The expectation value of the squared spin operator is never larger than 5% of the expected value at $E_{coll} = 0.65$ eV, though. Nevertheless, this small spin contamination leads to imperfections in the energy conservation of typically less than 1 kcal/mol. Smaller integration time steps in the equations of motion did not improve energy conservation because spin contamination is always present in the region of strong interaction, regardless of the integration time step.

One caveat with the MSINDO semiempirical Hamiltonian is that it overestimates the harmonic vibrational frequencies by ~20% compared with experiments or with more accurate calculations (see Table 5). Thus, in the microcanonical sampling of initial conditions for CH_4 reagents for the SRP-MSINDO and MSINDO surfaces, we provide 80% of the corresponding zero-point energy so that the energy above the barrier in calculations and experiments is the same.

A total of 120 000 trajectories have been calculated at $E_{coll} = 0.65$ eV with the MSINDO, SRP-MSINDO, and EG surfaces to compare with experiments.[33] Batches of ~20 000 trajectories have also been calculated for collision energies ranging from 0.6 to 1.2 eV with the three surfaces. Overall, the present calculations have involved $\sim 6 \times 10^8$ evaluations of energy gradients using electronic structure methods. Such a large number of energy gradients prohibits use of first-principles methods.

B. Comparison with Experiments. Figure 3 displays the OH rotational distributions calculated with the MSINDO, SRP-MSINDO, and EG PESs at $E_{coll} = 0.65$ eV, in comparison with the experiments of McKendrick and co-workers.[33] It should be noted that the experimental results correspond to the $^2\Pi_{3/2}$ state of OH. We have mapped the j' rotational states of the OH product in our quasiclassical trajectory calculations into N' total angular momentum quantum numbers (excluding the electronic and nuclear spin) using $N' = j' + 1$. The original MSINDO Hamiltonian greatly overestimates the experimental OH rotational distributions. The OH rotational distributions of the EG PES are also hotter than experiments. However, the SRP-MSINDO Hamiltonian developed here provides rotational distributions in remarkable agreement with experiments.

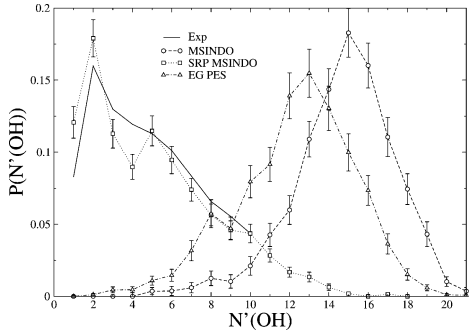

Figure 3. Calculated and experimental OH($v'=0$) rotational distributions. The calculations are carried out at $E_{coll} = 0.65$ eV. The experiments correspond to the $^2\Pi_{3/2}$ state of OH (ref 33). The experimental distribution is normalized so that the area under the 1−10 N′ states is identical with that of the SRP-MSINDO distribution in those rotational levels.

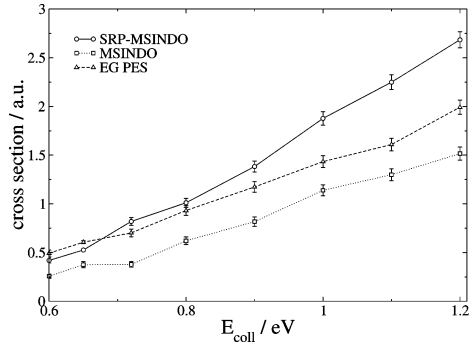

Figure 4. Excitation functions (cross sections vs collision energy) of the O(^{3}P) + CH_4 $\rightarrow$ OH + CH_3 reaction calculated with the SRP-MSINDO, MSINDO, and EG PES.

This result nicely demonstrates the relationship between potential energy surface and dynamics. The SRP-MSINDO Hamiltonian properly describes the regions of the potential energy surface explored in these calculations, and this leads to improved agreement with experimental results. On the other hand, the original MSINDO Hamiltonian fails to describe some regions of the potential energy surface, particularly the reaction energy, and this leads to a strong overestimation of rotational excitation. The EG PES was derived based on VTST thermal rate constants, and although this surface provides rate constants that are in quantitative agreement with experiments, it fails to describe regions of the surface near the minimum energy reaction path.

C. Excitation Functions. Figure 4 shows the excitation functions in the 0.6−1.2 eV collision-energy range. The reactive cross sections increase linearly with collision energy for the three surfaces. Whereas the cross sections for the MSINDO and SRP-MSINDO surfaces seem to converge at low energies, the slopes of the excitation functions are different, with SRP-MSINDO being more reactive at higher energies. As can be seen in Figure 2, both surfaces differ in the high-energy region, and this can be appreciated in the cross sections. The cross sections of the EG PES fall between the MSINDO and SRP-MSINDO cross sections at moderate and high energies, but seem to be larger at low energies. The maximum reactive impact parameters (b_{max}) also increase with collision energy in all surfaces. In the case of the SRP-MSINDO surface, b_{max} rises from 3.8 au at $E_{coll} = 0.6$ eV to 4.3 au at $E_{coll} = 1.2$ eV. The increase in reactive impact parameters with collision energy suggests that at energies well above the saddle point, the reaction is not confined to near-collinear approaches. Instead, an oxygen

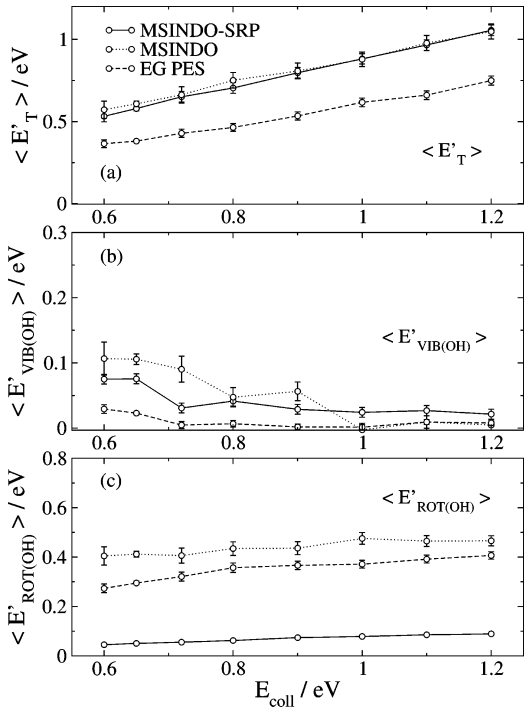

Figure 5. Average energy in products as a function of collision energy for the $O(^3P) + CH_4 \rightarrow OH + CH_3$ reaction using the SRP-MSINDO, MSINDO, and EG PES: (a) average products relative translational energy; (b) average OH vibrational energy; and (c) average OH rotational energy.

atom can abstract a hydrogen atom from methane with a more peripheral approach.

D. Energy Partitioning. Figure 5 shows a comparison of average product energies for the MSINDO, SRP-MSINDO, and EG surfaces. Most of the energy is channeled into products relative translational energy in all surfaces (Figure 5a). The results of the SRP-MSINDO and MSINDO surfaces overlap, and indicate a noticeably larger amount of energy going into translation than in the EG PES.

All three surfaces show that there is little energy released as OH vibration (Figure 5b). Thus, OH arises vibrationally cold, with residual populations of $\sim$10−20% in $v' = 1$ in all surfaces. Nonetheless, it can be noted that at low energies, the OH vibrational energy estimated by both the semiempirical surfaces is a bit larger than that in the EG PES. This result seems to slightly deviate from experiments,[33] which did not find appreciable population in the OH(v'=1) level. In earlier work,[25] it was mentioned that this behavior could be due to a variety of common pitfalls of the quasiclassical trajectory method, such as zero-point energy violation, absence of tunneling, or rounding off the classical vibrational actions to the nearest integer. Another issue likely responsible for the apparent overestimation of vibrational excitation of OH by the MSINDO and SRP-MSINDO Hamiltonians is tied to the characteristics of the molecular vibrations with this Hamiltonian. As mentioned before, both MSINDO and SRP-MSINDO overestimate the harmonic normal mode vibrational frequencies by $\sim$20%. The consequent stiffer nature of the OH stretch likely plays a role in the slightly enhanced amount of energy being channeled to this mode in these surfaces.

Regarding OH rotation (Figure 5c), the results of the SRP-MSINDO surface can be clearly distinguished from those of the MSINDO and EG PESs, as has been shown in the rotational distributions of Figure 3. MSINDO overestimates the energy available to products (see Table 1). In Figure 5, we see that the excess of energy available to products in the MSINDO trajectory calculations goes into rotation of the OH fragment. On the other hand, the EG PES describes correctly the reaction energetics, but furnishes overexcited OH rotational distributions. Figure 5 shows that the overly large OH rotational energy is related to a decrease in the amount of products translational energy relative to the more accurate SRP-MSINDO surface.

The methyl radical arises with energy below its zero point at all initial collision energies, and this happens for the MSINDO, SRP-MSINDO, and EG surfaces. Although this result is an artifact of the quasiclassical trajectory method, what we learn is that methyl does not receive a large amount of energy during the course of the reaction. This idea was initially suggested from the experiments of Suzuki and Hirota. That set of experiments indicated that at low energy, the population of the CH_3 umbrella mode was almost statistical.[32]

Figure 5 also shows the evolution of average product energies with collision energy. Interestingly, all three surfaces exhibit the same trends. The average values of product translational energy increase linearly with collision energy, with the slope being close to 1. This finding indicates that the amount of energy transferred into molecular modes is roughly constant at all collision energies, as can be seen in the evolution of the average OH vibrational and rotational energy with collision energy. Whereas the OH rotational energy seems to mildly increase with collision energy, the amount of energy going into OH vibration decays slightly. The fact that OH does not become vibrationally excited with increasing collision energy concurs with earlier calculations at hyperthermal energies with the MSINDO Hamiltonian. Those calculations showed that OH is vibrationally cold even when generated at collision energies of up to 5 eV,[25] demonstrating that the OH mode is uncoupled from the reaction coordinate. This behavior is at odds with earlier triatomic calculations that reported a moderate increase in OH vibrational excitation with increasing collision energy.[22]

E. Influence of Reagent Vibrational Excitation. We have also studied how initial vibrational excitation influences the dynamics of the $O(^3P) + CH_4 \rightarrow OH + CH_3$ reaction using the SRP-MSINDO, MSINDO, and EG surfaces. Classically, it is possible to assign an arbitrary amount of vibrational energy to methane. To compare the differences between reagent translation and reagent vibration, we have calculated a batch of 20 000 trajectories at $E_{coll} = 0.65$ eV with an amount of vibrational energy in methane corresponding to 0.589 quanta ($E_{VIB(CH_4)} = 1.73$ eV). These trajectories have the same total energy as the regular calculations described above at $E_{coll} = 1.2$ eV ($E_{VIB(CH_4)} = 1.18$ eV). Thus, comparison between both sets of calculations is intended to shed light on the differences in the dynamics when reagents are translationally or vibrationally excited.

Table 6 shows the enhancement factors of the cross section with $E_{coll} = 1.2$ eV, $E_{VIB(CH_4)} = 1.18$ eV, and $E_{coll} = 0.65$ eV, $E_{VIB(CH_4)} = 1.73$ eV, with respect to the cross section for $E_{coll} = 0.65$ eV, $E_{VIB(CH_4)} = 1.18$ eV. Both collision energy and vibrational excitation in methane enhance the reactive cross section. In all three surfaces, the cross section for the calculations with vibrationally excited methane is smaller than with translational excitation. This result suggests that, although vibrational excitation is somewhat coupled to the reaction coordinate, not all of the vibrational modes actively promote reactivity. The enhancement of reactivity by methane vibrational excitation is analogous in all surfaces. This behavior is to be compared with the differences in the enhancement of reactivity by translational excitation. As seen in Figure 4, the slope of the SRP-MSINDO surface excitation function is larger than that of the MSINDO

TABLE 6: Relative Cross Section and Average Fractions of Energy in Products as a Function of Initial Conditions for the $O(^3P) + CH_4 \rightarrow OH + CH_3$ Reaction Using the SRP-MSINDO, MSINDO, and EG Surfaces

surface	initial conditions	rel cross section[a]	$\langle f'_T \rangle$	$\langle f'_{VIB(OH)} \rangle$	$\langle f'_{ROT(OH)} \rangle$	$\langle f'_{INT(CH3)} \rangle$
SRP-MSINDO	$E_{coll} = 1.20$ eV, $E_{VIB(CH_4)} = 1.18$ eV	5.0	0.91 ± 0.03	0.02 ± 0.01	0.07 ± 0.01	0.00 ± 0.01
	$E_{coll} = 0.65$ eV, $E_{VIB(CH_4)} = 1.73$ eV	3.0	0.70 ± 0.03	0.19 ± 0.01	0.11 ± 0.01	0.00 ± 0.01
MSINDO	$E_{coll} = 1.20$ eV, $E_{VIB(CH_4)} = 1.18$ eV	4.3	0.69 ± 0.02	0.00 ± 0.01	0.31 ± 0.01	0.00 ± 0.01
	$E_{coll} = 0.65$ eV, $E_{VIB(CH_4)} = 1.73$ eV	3.2	0.48 ± 0.02	0.18 ± 0.01	0.31 ± 0.01	0.03 ± 0.01
EG PES	$E_{coll} = 1.20$ eV, $E_{VIB(CH_4)} = 1.18$ eV	3.3	0.64 ± 0.03	0.01 ± 0.01	0.35 ± 0.01	0.00 ± 0.01
	$E_{coll} = 0.65$ eV, $E_{VIB(CH_4)} = 1.73$ eV	2.9	0.41 ± 0.02	0.13 ± 0.01	0.30 ± 0.02	0.16 ± 0.01

[a] Ratio of the cross section at the specified conditions over the cross section at $E_{coll} = 0.65$ eV, $E_{CH_4} = 1.18$ eV.

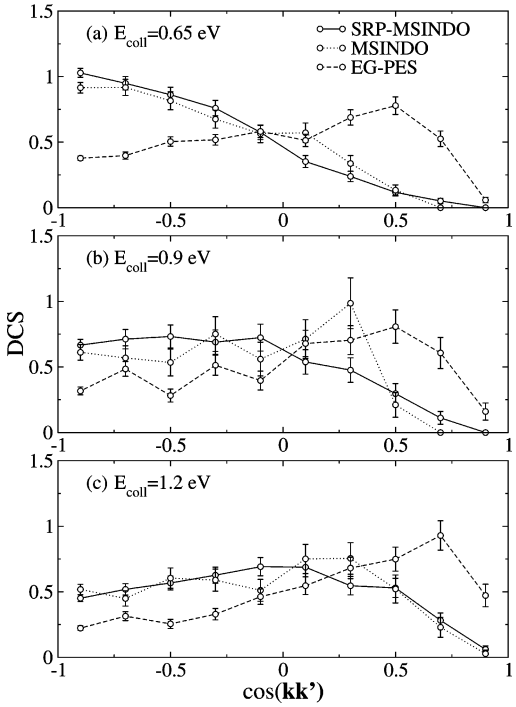

Figure 6. **kk′** angular distributions expressed as differential cross sections (DCS, $2\pi/\sigma\ d\sigma/d\Omega'$) for the $O(^3P) + CH_4 \rightarrow OH + CH_3$ reaction using the SRP-MSINDO, MSINDO, and EG PES: (a) $E_{coll} = 0.65$ eV; (b) $E_{coll} = 0.9$ eV; and (c) $E_{coll} = 1.2$ eV.

surface. The data in Table 6 corroborate the larger reactivity of the SRP-MSINDO surface. The increase in reactivity by translational excitation is more moderate with EG PES than with the other two surfaces. Thus, for the EG PES, the vibrational and translational enhancement factors become comparable.

Table 6 also shows the average fractions of energy in products. Clearly, initial vibrational excitation increases the amount of energy released to OH vibration at the expense of product translation. OH rotation seems independent of increases in the amount of vibrational excitation initially present in methane. The amount of internal energy in the methyl product increases when methane is vibrationally excited with respect to calculations with methane having zero-point energy but more translational excitation. However, the fractions of energy in the SRP-MSINDO and MSINDO surfaces remain close to zero because the amount of energy going into methyl vibration is still below the zero point.

In the future, it will be interesting to develop mode-specific studies in which individual vibrations of methane are excited, instead of exciting all of the vibrational modes. This will allow us to derive full-dimensional state-to-state knowledge of this benchmark reaction.

F. Angular Distributions. Figure 6 shows **kk′** angular distributions in terms of solid-angle differential cross sections at three collision energies for the SRP-MSINDO, MSINDO, and EG surfaces. (**k** is the reagent's relative velocity vector pointing from O to CH_4, and **k′** is the product's relative velocity vector pointing from CH_3 to OH.) At $E_{coll} = 0.65$ eV, the distributions are dominated by backward scattering in the SRP-MSINDO and MSINDO surfaces. Backward scattering is expected at low energies from the near-collinear geometry of the saddle point. However, the angular distributions of the EG PES are not as backward as those calculated with the semiempirical surfaces, indicating a broader cone of acceptance of the prior surface. The angular distributions broaden with increasing collision energy. This result reinforces the idea that larger collision energies enable the system to explore regions of the potential energy surface removed from the minimum energy reaction path. However, even at $E_{coll} = 1.2$ eV, ~60% of the flux is still confined in the backward hemisphere for the SRP-MSINDO surface. This suggests that although the cone of acceptance broadens with increasing collision energy, the potential energy surface of the title reaction is very anisotropic in this surface. Earlier calculations with the original MSINDO Hamiltonian showed that forward scattering is observed only at collision energies well above 3 eV.[25]

Concluding Remarks

The $O(^3P) + CH_4 \rightarrow OH + CH_3$ reaction has been studied with electronic structure, VTST, and quasiclassical-trajectory calculations. Electronic structure calculations indicate that the PMP2//UMP2/AUG-cc-pVDZ model chemistry reasonably describes the reaction energies and barriers in comparison with more accurate methods. Using a grid of 728 ab initio points at that level, we reoptimize the parameters of the MSINDO semiempirical Hamiltonian to obtain a specific reaction parameters MSINDO surface that is able to produce accurate energies for the title reaction at a reduced computational cost. The SRP-MSINDO Hamiltonian clearly improves the performance of the original Hamiltonian, providing reaction energies, barriers, and saddle point geometries in agreement with more accurate but more expensive calculations.

Although we have focused our efforts on describing regions of the potential energy surface outside the minimum energy reaction path, Variational Transition State Theory calculations of the thermal rate constants show that the SRP-MSINDO semiempirical Hamiltonian yields rate constants in agreement with experiments. Quasiclassical trajectory studies indicate that the SRP-MSINDO surface is also accurate in regions beyond the minimum energy reaction path. The $OH(v'=0)$ rotational distributions obtained with the SRP-MSINDO PES agree with experiments, clearly improving over the results with the original Hamiltonian and the prior EG PES.

Additional trajectories are propagated by using the SRP-MSINDO, MSINDO, and EG surfaces to gain further insight on the reaction dynamics, and learn the correlation between surface topology and dynamics. Both SRP-MSINDO and

MSINDO surfaces give similar average energies for product translation and OH vibration, but MSINDO greatly overestimates the rotational excitation of the OH product. The EG PES also overestimates the amount of energy released as OH rotation, at the expense of a decreased energy release to product translation. All three surfaces yield vibrationally cold OH, with both semiempirical surfaces predicting average OH vibrational energy slightly above the EG PES results at low collision energies. Increases in collision energy do not lead to increases in the amount of energy released to OH or CH_3 molecular modes. On the other hand, initial vibrational excitation of methane promotes internal excitation of the OH product at the expense of product translation for all three surfaces.

The results presented in this paper indicate that reparametrization of semiempirical Hamiltonians can be a suitable approach to generate accurate potential energy surfaces for gas-phase polyatomic reactions. Although direct-dynamics studies are traditionally daunting, improved semiempirical Hamiltonians enable calculation of hundreds of thousands of trajectories for systems such as the one studied in this work.

Acknowledgment. This work has been supported by a new faculty start-up allowance from the Department of Chemistry at Virginia Tech.

References and Notes

(1) Mielke, S. L.; Peterson, K. A.; Schwenke, D. W.; Garrett, B. C.; Truhlar, D. G.; Michael, J. V.; Su, M. C.; Sutherland, J. W. *Phys. Rev. Lett.* **2003**, *91*, 063201.

(2) Zhang, D. H.; Collins, M. A.; Lee, S. Y. *Science* **2000**, *290*, 961.

(3) Troya, D.; Lakin, M. J.; Schatz, G. C. Quasiclassical trajectory studies of four-atom reactions. In *Modern Trends in Chemical Reaction Dynamics. Experiment and Theory* (*Part I*); Yang, X., Liu, K., Eds.; World Scientific: River Edge, NJ, 2004; p 249.

(4) Collins, M. A. *Theor. Chem. Acc.* **2002**, *108*, 313.

(5) Wu, T.; Manthe, U. *J. Chem. Phys.* **2003**, *119*, 14.

(6) Wu, T.; Werner, H.-J.; Manthe, U. *Science* **2004**, *306*, 2227.

(7) Sierra, J. D.; Enriquez, P. A.; Troya, D.; Gonzalez, M. *Chem. Phys. Lett.* **2004**, *399*, 527.

(8) Bolton, K.; Hase, W. L. Direct dynamics simulations of reactive systems. In *Modern Methods for Multidimensional Dynamics Computations in Chemistry*; Thompson, D. L., Ed.; World Scientific: Singapore, 1998; p 143.

(9) Troya, D.; Schatz, G. C. *J. Chem. Phys.* **2004**, *120*, 7696.

(10) Gonzalez-Lafont, A.; Truong, T. N.; Truhlar, D. G. *J. Phys. Chem.* **1991**, *95*, 4618.

(11) Li, G.; Bosio, S. B. M.; Hase, W. L. *J. Mol. Struct.* **2000**, *556*, 43.

(12) Warnatz, J. In *Combustion Chemistry*; Gardiner, W. C., Jr., Ed.; Springer-Verlag: Berlin, Germany, 1984; p 197.

(13) Wang, M.-L.; Li, Y.-M.; Zhang, J. Z. H. *J. Phys. Chem. A* **2001**, *105*, 2530.

(14) Yu, H.-G.; Nyman, G. *J. Chem. Phys.* **2000**, *112*, 238.

(15) Palma, J.; Clary, D. C. *J. Chem. Phys.* **2000**, *112*, 1859.

(16) Palma, J.; Clary, D. C. *Phys. Chem. Chem. Phys.* **2000**, *2*, 4105.

(17) Palma, J.; Clary, D. C. *J. Chem. Phys.* **2001**, *115*, 2188.

(18) Huarte-Larranaga, F.; Manthe, U. *J. Chem. Phys.* **2002**, *117*, 4635.

(19) Espinosa-Garcia, J.; Garcia-Bernaldez, J. C. *Phys. Chem. Chem. Phys.* **2000**, *2*, 2345.

(20) Truhlar, D. G.; Isaacson, A. D.; Garrett, B. C. Generalized transition state theory. In *The Theory of Chemical Reaction Dynamics*; Baer, M., Ed.; CRC Press: Boca Raton, FL, 1985; Vol. 4, p 65.

(21) Gonzalez, M.; Hernando, J.; Millan, J.; Sayos, R. *J. Chem. Phys.* **1999**, *110*, 7326.

(22) Sayós, R.; Hernando, J.; Puyuelo, M. P.; Enríquez, P. A.; González, M. *Chem. Phys. Lett.* **2003**, *341*, 608.

(23) Troya, D.; Millan, J.; Banos, I.; Gonzalez, M. *J. Chem. Phys.* **2002**, *117*, 5730.

(24) Troya, D.; Millan, J.; Banos, I.; Gonzalez, M. *J. Chem. Phys.* **2004**, *120*, 5181.

(25) Troya, D.; Pascual, R. Z.; Schatz, G. C. *J. Phys. Chem. A* **2003**, *107*, 10497.

(26) Troya, D.; Schatz, G. C. Dynamics studies of the $O(^3P) + CH_4$, C_2H_6 and C_3H_8 reactions. In *Theory of Chemical Reaction Dynamics*; Lagana, A., Lendvay, G., Eds.; Kluwer Academic Publishers: Dordrecht, The Netherlands, 2004; p 329.

(27) Troya, D.; Schatz, G. C.; Garton, D. J.; Brunsvold, A. L.; Minton, T. K. *J. Chem. Phys.* **2004**, *120*, 731.

(28) Troya, D.; Schatz, G. C. *Int. Rev. Phys. Chem.* **2004**, *23*, 341.

(29) Garton, D. J.; Minton, T. K.; Troya, D.; Pascual, R.; Schatz, G. C. *J. Phys. Chem. A* **2003**, *107*, 4583.

(30) Stewart, J. J. P. *J. Comput. Chem.* **1989**, *10*, 209.

(31) Ahlswede, B.; Jug, K. *J. Comput. Chem.* **1999**, *20*, 563.

(32) Suzuki, T.; Hirota, E. *J. Chem. Phys.* **1993**, *98*, 2387.

(33) Sweeney, G. M.; Watson, A.; McKendrick, K. G. *J. Chem. Phys.* **1997**, *106*, 9172.

(34) Sweeney, G. M.; Watson, A.; McKendrick, K. G. *J. Chem. Phys.* **1997**, *106*, 9182.

(35) Ausfelder, F.; Kelso, H.; McKendrick, K. G. *Phys. Chem. Chem. Phys.* **2002**, *4*, 473.

(36) McFarlane, J.; Polanyi, J. C.; Shapter, J. G. *J. Photochem. Photobiol. A* **1991**, *58*, 139.

(37) Corchado, J. C.; Espinosa-Garcia, J.; Roberto-Neto, O.; Chuang, Y.-Y.; Truhlar, D. G. *J. Phys. Chem. A* **1998**, *102*, 4899.

(38) Roberto-Neto, O.; Machado, F. B. C.; Truhlar, D. G. *J. Chem. Phys.* **1999**, *111*, 10046.

(39) Yan, T.; Hase, W. L.; Doubleday: C. *J. Chem. Phys.* **2004**, *120*, 9253.

(40) Yan, T.; Doubleday: C.; Hase, W. L. *J. Phys. Chem. A* **2004**, *108*, 9863.

(41) Frisch, M. J.; Trucks, G. W.; Schlegel, H. B.; Scuseria, G. E.; Robb, M. A.; Cheeseman, J. R.; Montgomery, J. A., Jr.; Vreven, T.; Kudin, K. N.; Burant, J. C.; Millam, J. M.; Iyengar, S. S.; Tomasi, J.; Barone, V.; Mennucci, B.; Cossi, M.; Scalmani, G.; Rega, N.; Petersson, G. A.; Nakatsuji, H.; Hada, M.; Ehara, M.; Toyota, K.; Fukuda, R.; Hasegawa, J.; Ishida, M.; Nakajima, T.; Honda, Y.; Kitao, O.; Nakai, H.; Klene, M.; Li, X.; Knox, J. E.; Hratchian, H. P.; Cross, J. B.; Bakken, V.; Adamo, C.; Jaramillo, J.; Gomperts, R.; Stratmann, R. E.; Yazyev, O.; Austin, A. J.; Cammi, R.; Pomelli, C.; Ochterski, J. W.; Ayala, P. Y.; Morokuma, K.; Voth, G. A.; Salvador, P.; Dannenberg, J. J.; Zakrzewski, V. G.; Dapprich, S.; Daniels, A. D.; Strain, M. C.; Farkas, O.; Malick, D. K.; Rabuck, A. D.; Raghavachari, K.; Foresman, J. B.; Ortiz, J. V.; Cui, Q.; Baboul, A. G.; Clifford, S.; Cioslowski, J.; Stefanov, B. B.; Liu, G.; Liashenko, A.; Piskorz, P.; Komaromi, I.; Martin, R. L.; Fox, D. J.; Keith, T.; Al-Laham, M. A.; Peng, C. Y.; Nanayakkara, A.; Challacombe, M.; Gill, P. M. W.; Johnson, B.; Chen, W.; Wong, M. W.; Gonzalez, C.; Pople, J. A. *Gaussian 03*, Revision C.02; Gaussian Inc.: Wallingford, CT, 2004.

(42) NIST Computational Chemistry Comparison and Benchmark Database, http://srdata.nist.gov/cccbdb, IV. A.1 Reaction Comparison. Experimental Enthalpies at 0 K.

(43) Schlegel, H. B. *J. Phys. Chem.* **1988**, *92*, 3075.

(44) www.netlib.org.

(45) Cohen, N. *Int. J. Chem. Kinet.* **1986**, *18*, 59.

(46) Sutherland, J. W.; Michael, J. V.; Klemm, R. B. *J. Phys. Chem.* **1986**, *90*, 5941.

(47) Cohen, N.; Westberg, K. R. *J. Phys. Chem. Ref. Data* **1991**, *20*, 1211.

(48) Baulch, D. L.; Cobos, C. J.; Cox, R. A.; Esser, C.; Frank, P.; Just, T.; Kerr, J. A.; Pilling, M. J.; Troe, J.; Walker, R. W.; Warnatz, J. *J. Phys. Chem. Ref. Data* **1992**, *21*, 445.

(49) Corchado, J. C.; Chuang, Y.-Y.; Fast, P. L.; Villà, J.; Hu, W.-P.; Liu, Y.-P.; Lynch, G. C.; Nguyen, K. A.; Jackels, C. F.; Melissas, V. S.; Lynch, B. J.; Rossi, I.; Coitiño, E. L.; Fernandez-Ramos, A.; Pu, J.; Albu, T. V.; Steckler, R.; Garrett, B. C.; Isaacson, A. D.; Truhlar, D. G. *POLYRATE* version 9.1, 2002.

(50) Page, M.; McIver, J. W. *J. Chem. Phys.* **1988**, *88*, 922.

(51) Hase, W. L.; Duchovic, R. J.; Hu, X.; Komornicki, A.; Lim, K. F.; Lu, D.-H.; Peslherbe, G. H.; Swamy, K. N.; vande Linde, S. R.; Varandas, A. J. C.; Wang, H.; Wolf, R. J. *VENUS96*, A general chemical dynamics computer program, 1996.